Topological Corner States due to Boundary Defects

Yiqi Zhang(张贻齐)[1*], Yuwei Hu(胡玉伟)[1], Yongdong Li(李永东)[1], and Ce Shang(尚策)[2,3*]

[1]*Key Laboratory for Physical Electronics and Devices, Ministry of Education, School of Electronic Science and Engineering, Xi'an Jiaotong University, Xi'an 710049, China*
[2]*Aerospace Information Research Institute, Chinese Academy of Sciences, Beijing 100094, China*
[3]*College of Precision Instrument and Optoelectronics Engineering, Tianjin University, Tianjin 300072, China*

(Received 1 November 2025; accepted manuscript online 3 December 2025)

In conventional higher-order topological insulators (HOTIs), the emergence of topological states can be explained by using the nonzero bulk polarization index. However, corner states emerge in HOTIs with incomplete boundary unit cells (i.e., boundary defects) even though the bulk polarization is zero, which challenges the conventional understanding of HOTIs. Here, based on a Kekulé-distorted honeycomb lattice with incomplete unit cells, we reveal that incomplete unit cells exhibit fractional charges through the analysis of Wannier centers by developing a compensation method and creating the concept of Wannier center domain (WCD) which is the smallest region that one Wannier center occupies. This method compensates for the missing parts of these boundary incomplete unit cells with additional WCDs to make them complete. The compensated WCDs automatically carry the corresponding charge, and this charge together with that of the incomplete unit cell constitutes the total charge of the complete unit cell after compensation. We conclude that the emergence of corner states is attributed to the filling anomaly, which is a fundamental mechanism. Our results refresh the understanding of HOTIs, especially those with structural discontinuities, and provide a novel design for topological states which have application value in producing optical functional devices.

DOI: 10.1088/0256-307X/43/1/010403 CSTR: 32039.14.0256-307X.43.1.010403

1. Introduction. The higher-order topological insulator (HOTI) is a specific material with the dimension of the topological state smaller than that of the underlying system at least by two.[1,2] In a two-dimensional (2D) HOTI, the topological corner state is a 0D state, which has been reported in a variety of systems.[3–14] Different from the topological invariant number—the Chern number, which is used for evaluating Chern insulator,[15] the HOTI does not comply with the bulk-edge correspondence principle[15] in Chern insulators, and its topological phase transition is generally described by the bulk polarization index[1]—a nonzero value indicates the appearance of the corner states. However, this bulk polarization index is only valid for lattices with complete unit cells.

According to the previous literature, the appearance of the corner state is due to the "filling anomaly"—a concept borrowed from solid state physics. The filling anomaly describes a mismatch that appears between the number of electrons in an energy band and the number of electrons required for charge neutrality,[3,16–18] which leads to the "fractional charges" in the corner unit cells of the lattice system. The concept of "fractional charge" is also adopted from solid state physics, and its analog in optical systems is the "spectral charge", characterizing the "number of modes" or "occupied sites" in the unit cell of the lattice that can be calculated using all states below the bandgap. Thus, by summing all states (normalized field intensity) below the considered bandgap, one may find that the resulting sum distributes uniformly over all sites in bulk unit cells (i.e., all sites in the bulk unit cells are occupied), but only over a few sites in boundary unit cells, with other sites being vacant. This summation also reflects the density of states in each unit cell, which helps understand the "filling anomaly". Since incomplete unit cells are artificially created, the "filling anomaly" in corner unit cells may be affected not only by Kekulé distortion operation[4,19] but also by missing sections of the unit cells. Therefore, we believe that the ultimate reason for the appearance of corner states is due to "filling anomaly" in lattice systems, regardless of whether a unit cell is complete or not. In addition, these corner states are protected by some symmetries; e.g., rotational symmetry. The bulk polarization index is only valid for systems with complete unit cells. This phenomenon cannot be illustrated by simple Su–Schrieffer–Heeger model where a unit cell can be redefined if one takes on trivial phase and breaks boundary unit cells such that they render edge state topological; although under original definitions the bulk polarization or winding number is zero. In a 2D sample, a unit cell cannot be redefined to include the dangling sites into more appropriate unit cell.

In this Letter, we conduct our discussion based on the well-known Kekulé distorted honeycomb lattice[4] by removing some sites from the unit cells at the edges and corners. We will show that the appearance of corner states in this lattice contradicts the theoretical prediction according

*Corresponding authors. Email: zhangyiqi@xjtu.edu.cn; shangce@aircas.ac.cn

to the bulk invariant that is followed traditionally.[3,4,20] We develop a fractional charge theory based on the filling anomaly, which is a generally feasible approach. The incomplete unit cells support fractional charges, defined when they are compensated by adjacent virtual lattice sections to form a complete effective unit. We introduce the concept of Wannier center domains (WCDs) to unify the description of charge redistribution in both topologically trivial and nontrivial regimes. The results lay the foundation for HOTIs with incomplete unit cells and refine the fractional charge theory for explaining the appearance of corner states.

2. Lattice with Incomplete Unit Cells. The Kekulé distorted honeycomb lattice with incomplete unit cells is shown in Fig. 1. The dashed part of the unit cell is missing, with the region highlighted with solid lines left. In consideration of the Kekulé distortion, we show two kinds of honeycomb lattices: one with intra-cell coupling greater than inter-cell coupling, shown in Fig. 1(a), and the other with intra-cell coupling less than inter-cell coupling, shown in Fig. 1(b). As shown in previous literature,[4] the corner states can only appear in the case shown in Fig. 1(b), since the bulk invariant for this case is nonzero. However, this is not correct here.

To seek the spectrum of the lattice in optical platforms, we adopt a continuous model that involves all necessary couplings among sites. We assume that the lattice is fabricated from fused silica material using the femtosecond laser direct writing technique,[8,11,12,20–23] and the propagation of the light beam can be described by the Schrödinger-like paraxial wave equation,

$$\mathrm{i}\frac{\partial\psi}{\partial z} = -\frac{1}{2}\nabla^2\psi - \mathcal{R}(x,y)\psi, \tag{1}$$

where $\nabla^2 \equiv \partial_x^2 + \partial_y^2$ is the transverse Laplacian; the transverse (x, y) and longitudinal z coordinates are dimensionless, and the function $\mathcal{R}(x, y)$ describes a shallow optical potential defining the lattice,

$$\mathcal{R}(x,y) = p\sum_{m,n}\exp[-(\boldsymbol{\rho}-\boldsymbol{\rho}_{m,n})^2/d^2],$$

where p is the depth of the potential, proportional to the depth of the refractive index modulation; $\boldsymbol{\rho}_{m,n} = (x_{m,n}, y_{m,n})$ are the grid coordinates of the sites that vary according to the shift parameter r—the separation between the six sites in each hexagonal unit cell; the side length of the unit cell is $\sqrt{3}a$; and d is the site width. If $r < a$, the intra-cell coupling is greater than the inter-cell coupling. Otherwise, the inter-cell coupling is greater than the intra-cell coupling. The solution of Eq. (1) has the form $\psi = u(x, y)\exp(ibz)$ with b being the propagation constant, so one obtains the eigenvalue problem,

$$bu = \frac{1}{2}\nabla^2 u + \mathcal{R}u,$$

which can be solved directly by using the plane-wave expansion method or the finite-difference method in real space. Since the lattice structure is finite-sized, the open

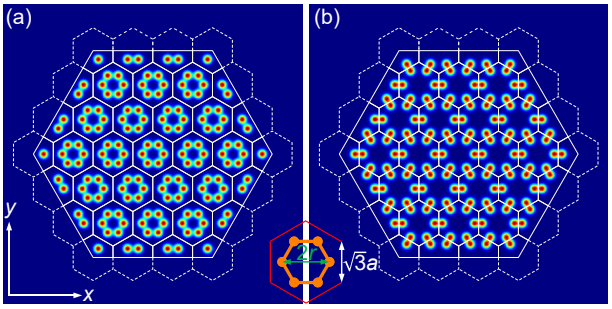

Fig. 1. Kekulé patterned honeycomb lattice with incomplete cells. The missed section of the cell is indicated by dashed lines. (a) Intra-cell coupling is greater than inter-cell coupling. (b) Inter-cell coupling is greater than intra-cell coupling.

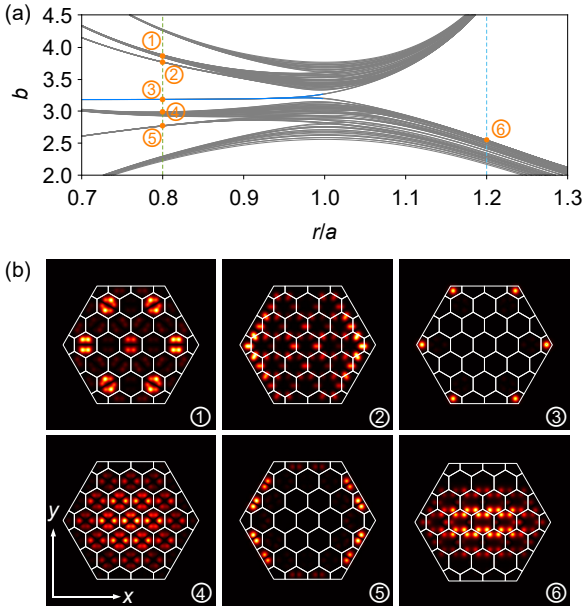

Fig. 2. (a) Spectrum of the Kekulé patterned honeycomb lattice with incomplete unit cells as a function of r which adjusts the separation between six sites in each unit cell. The blue line represents the corner state, while the gray lines represent the bulk or edge states. (b) Field modulus profiles of the states indicated with numbers in (a). Here, the normalized color scale is adopted. Parameters are $p = 10$, $d = 0.5$, and $a = 1.6$.

boundary condition for this problem is natural and direct. By adjusting the value of r, the spectrum of the Kekulé distorted honeycomb lattice with incomplete unit cells is shown in Fig. 2(a). One finds that there are no states in the band gap if $r > a$ (i.e., the inter-cell coupling is greater), while there are many states if $r < a$ (i.e., the intra-cell coupling is greater). The corner state is indicated by the blue line. The result in Fig. 2(a) is evidently distinct from that of the lattice with complete unit cells. To show the landscape of the states explicitly, we specifically choose 6 states as numbered in Fig. 2(a) and show their field modulus profiles in Fig. 2(b). The state numbered 3 from the blue line is the corner state, which is six-fold degenerate. The state numbered 5 is an edge state, while the other states are bulk states. Again, we would like to empha-

size that neither corner states nor edge states here can be explained by the bulk invariant previously developed.

3. Mode Density and Fractional Charge. The fractional charge here refers to the spectral charge, which accounts for the state carried per unit cell. The spectral charge for each unit cell can be obtained by superimposing the field intensity of all the normalized eigenstates below the corner state [cf. the blue line in Fig. 2(a)]. Since the superimposed result reflects the number of states for each unit cell, it also indicates the mode density, which can be obtained via

$$\mathcal{D}(x,y)=\int_{b_{\min}}^{b_{\max}}|u_b(x,y)|^2\mathrm{d}b,$$

where $u_b(x,y)$ is the normalized eigenstate with propagation constant b that $\iint|u_b(x,y)|^2\mathrm{d}x\mathrm{d}y=1$, and the integration region is $b_{\min}<b<b_{\max}$ with $b_{\max}$ being the propagation constant of the corner state and $b_{\min}$ the propagation constant of the lowest bulk state. For the case with $r<a$, the mode density distribution is shown in Fig. 3(a). One finds that the unit cells, except for those at the boundaries and corners, are almost uniformly occupied. In Fig. 3(b), we show the fractional charge in each unit cell, including the incomplete ones, which is obtained via

$$\mathcal{Q}=\frac{\int_S\mathcal{D}(x,y)\mathrm{d}x\mathrm{d}y}{\int_{S_{\mathrm{norm}}}\mathcal{D}(x,y)\mathrm{d}x\mathrm{d}y},$$

where S is the area of each (incomplete) unit cell and S_{norm} is the area of the unit cell that is used to do normalization. Indeed, the value for the bulk unit cell is ~1 and that for the incomplete unit cell is ~0. Note that the value in the middle unit cell is lower than that in its surrounding unit cells, but it is still close to 1 and does not affect the general result.

For the case with $r>a$, the mode density distribution and the corresponding fractional charge in each unit cell are shown in Figs. 3(c) and 3(d), respectively. Since there is no corner state in the band gap for this case, we set $b_{\max}$ to be the propagation constant of the uppermost bulk state below the band gap. One finds that the bulk unit cells are almost uniformly occupied, which is expected, but there are also states in the corners and edges of incomplete unit cells, which are different from the case shown in Fig. 3(a). As displayed in Fig. 3(d), the fractional charge of the incomplete unit cell in the corners is close to 1/6, while that of the incomplete unit cell at the edges is close to 1/3. Clearly, the fractional charges shown in Fig. 3 still cannot explain the appearance of corner states in Fig. 2. Before solving this problem, we would like to first introduce the Wannier center method. We would like to note that the mode density in Fig. 3 is not $\mathcal{C}_6$ symmetric even though the lattice is. This mismatch between the lattice symmetry and the boundary geometry introduces finite-size effects that slightly break the rotational symmetry in the numerical results.

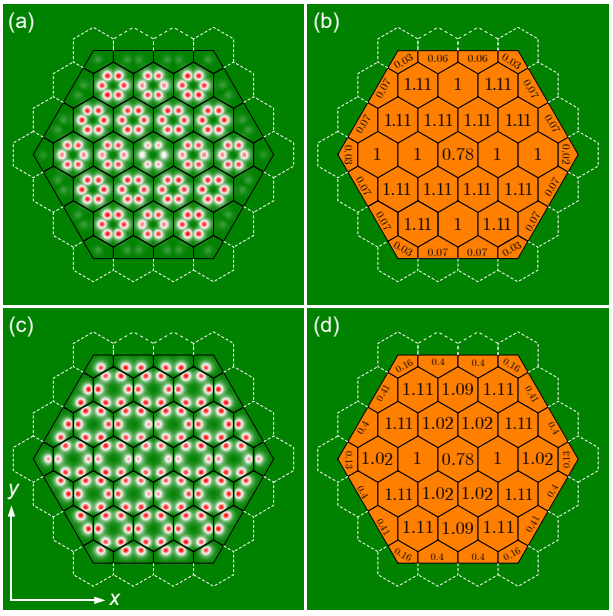

Fig. 3. (a) Mode density in the Kekulé patterned honeycomb lattice with incomplete unit cells and $r/a=0.8$. (b) The fractional charge in each unit cell based on the mode density in (a). (c) Similar to that shown in (a) but for $r/a=1.2$. (d) The fractional charge in each unit cell based on the mode density in (c). The color scale in (a) and (c) is normalized.

4. Wannier Center, Fractional Charge, and Corner States. The Wannier center indicates the average position of the electrons.[3] If $r<a$, the Wannier centers are located at the center of the unit cell [cf. red dots in Fig. 4(a)]; otherwise, they are at the midpoint of the cell edges [cf. red dots in Fig. 4(b)]. According to the relation between the Wannier center and the fractional charge, the charge in the bulk unit cell is 1, and the charge in the corner and edge incomplete unit cells is 0 in Fig. 4(a). The charge in the corner incomplete unit cell in Fig. 4(b) is 1/6, and that in the edge incomplete unit cell is 1/3. The results in Fig. 4 are consistent with those in Fig. 3. Therefore, the Wannier center method can be used for subsequent analysis.

To explain the appearance of the corner state in the incomplete corner unit cell, we would like to introduce a new viewpoint that the charge should be considered in a complete cell, and the appearance of the corner state cannot be predicted from the charge of the incomplete unit cell only. To this end, one has to consider the sections with dashed edges. That is to say, the incomplete unit cell should be compensated, and then the total charge of the compensated complete unit cell can be calculated. To illustrate the viewpoint clearly, we first take the top-left corner unit cell in Fig. 4(a) as an example. One takes a unit cell that has a charge of 1 to compensate for the corner unit cell, since the blue sector is already there, one has to compensate the left sector with dashed edges to complete the corner incomplete unit cell. The Wannier center is then cut, leading to the fractional charge of the unit cell. As shown in Fig. 4(c), the charge of the unit cell after compensation is 2/3, which equals 1 minus the ratio

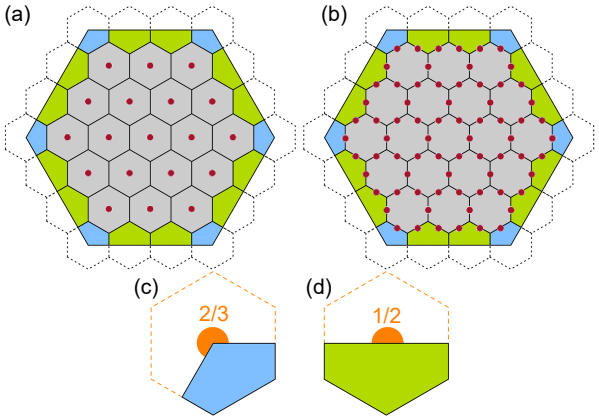

Fig. 4. (a) Wannier center (red dots) in the Kekulé patterned honeycomb lattice with incomplete unit cells and $r/a = 0.8$. (b) Same as (a) but for the case with $r/a = 1.2$. (c) Partial Wannier center in the incomplete corner unit cells after compensation for $r/a = 0.8$. (d) Same as (c) but for the incomplete edge unit cell.

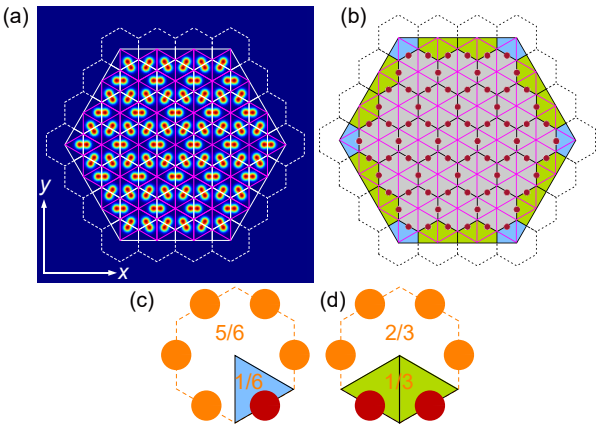

Fig. 5. (a) Lattice with $r/a = 1.2$ and with the WCDs indicated by magenta rhombuses. (b) Same as that in Fig. 4(b) with the WCDs indicated by magenta rhombuses. (c) The compensated Wannier centers (orange dots) and original Wannier center (red dot) for the incomplete corner unit cell. (d) Same as (c) but for the incomplete edge unit cell.

between the incomplete unit cell area (blue area) and the unit cell area (viz. $1 - 1/3 = 2/3$). Similarly, the charge of the incomplete edge unit cell after compensation is $1/2$, as shown in Fig. 4(d). The fractional charge indicates the appearance of the corner states in the lattice with $r < a$, even though the corresponding bulk invariant is zero. However, for the case with $r > a$, the situation is a bit complex. We would like to define a new concept—Wannier center domain (WCD) that describes the function area of the Wannier center:

- If $r < a$, the Wannier center is in the center of the unit cell, and the WCD overlaps with the unit cell;
- If $r > a$, the WCD does not overlap with the unit cell any longer, and it becomes rhombic. The unit cell is the simplest repeating unit of the lattice, but the WCD is not.

As shown in Fig. 5(a), we project the WCD onto the lattice in Fig. 1(b) by using magenta rhombuses together with hexagonal unit cells. For the corresponding Wannier centers shown in Fig. 4(b), we also display the magenta WCD rhombuses, as shown in Fig. 5(b). In this way, the Wannier centers are in their own WCDs as those in Fig. 4(a). The introduction of WCD is straightforward and natural because it is centered on the Wannier centers. For the case $r > a$, as shown in Figs. 5(a) and 5(b), the area of the hexagonal unit cell is three times that of the rhombic WCD. Also, take the top-left corner incomplete unit cell as our analysis object, as shown in Fig. 5(b), which includes one-half of a rhombic WCD. Therefore, one has to compensate for the incomplete unit cell by using five additional WCDs, each with one Wannier center. The incomplete corner unit cell after compensation is illustrated in Fig. 5(c), with six Wannier centers localized at the midpoints of the edges of the unit cell. Five of the Wannier centers indicated with orange color are from compensation, and the red one in the blue region (i.e., half of the WCD) is the original one. As a result, the total charge of the corner unit cell after compensation is 1, which is not fractional and indicates the impossible appearance of the corner states. The incomplete edge unit cells can be analyzed in a similar way.

5. Conclusion and Outlook. In conclusion, we have reported WCD-characterized HOTIs with incomplete unit cells (that can be classified into topological defects[2]) which are governed by fractional charges. By analyzing the Kekulé-distorted honeycomb lattice truncated through incomplete unit cells, we revealed that fractional charges in boundary regions arise from the compensation of incomplete unit cells by adjacent virtual lattice sections. We would like to emphasize that all the phenomena reported in this work can be experimentally demonstrated in a waveguide array fabricated in the fused silica material by using the femtosecond laser direct writing technique. These findings reconcile the apparent contradiction between bulk invariants and boundary phenomena in structurally discontinuous systems. This work opens several promising avenues for the exploration of the same concept in three-dimensional systems,[24,25] systems with fractal dimensions,[12,26,27] quasicrystals,[28] moiré lattices,[29–33] topological circuits,[34] to name a few. By bridging the gap between ideal crystal models and real-world structural imperfections, the framework may inspire topological device designs with on-chip application value.[35,36]

Acknowledgements. This work was supported by the Natural Science Basic Research Program of Shaanxi Province (Grant Nos. 2024JC-JCQN-06 and 2025JC-QYCX-006), the National Natural Science Foundation of China (Grant No. 12474337), and Chinese Academy of Sciences Project (Grant Nos. E4BA270100, E4Z127010F, E4Z6270100, and E53327020D).

References

[1] Xie B, Wang H X, Zhang X, Zhan P, Jiang J H, Lu M, and Chen Y 2021 *Nat. Rev. Phys.* **3** 520

[2] Lin Z K, Wang Q, Liu Y, Xue H, Zhang B, Chong Y, and Jiang J H 2023 *Nat. Rev. Phys.* **5** 483

[3] Benalcazar W A, Li T, and Hughes T L 2019 *Phys. Rev. B* **99** 245151

[4] Noh J, Benalcazar W A, Huang S, Collins M J, Chen K P, Hughes T L, and Rechtsman M C 2018 *Nat. Photon.* **12** 408

[5] Chen X D, Deng W M, Shi F L, Zhao F L, Chen M, and Dong J W 2019 *Phys. Rev. Lett.* **122** 233902

[6] Xie B Y, Su G X, Wang H F, Su H, Shen X P, Zhan P, Lu M H, Wang Z L, and Chen Y F 2019 *Phys. Rev. Lett.* **122** 233903

[7] Zhang Y, Kartashov Y V, Torner L, Li Y, and Ferrando A 2020 *Opt. Lett.* **45** 4710

[8] Kirsch M S, Zhang Y, Kremer M, Maczewsky L J, Ivanov S K, Kartashov Y V, Torner L, Bauer D, Szameit A, and Heinrich M 2021 *Nat. Phys.* **17** 995

[9] Jin M C, Gao Y F, Lin H Z, He Y H, and Chen M Y 2022 *Phys. Rev. A* **106** 013510

[10] Zhang Y, Bongiovanni D, Wang Z, Wang X, Xia S, Hu Z, Song D, Jukić D, Xu J, Morandotti R, Buljan H, and Chen Z 2023 *eLight* **3** 5

[11] Arkhipova A A, Zhang Y, Kartashov Y V, Zhuravitskii S A, Skryabin N N, Dyakonov I V, Kalinkin A A, Kulik S P, Kompanets V O, Chekalin S V, and Zadkov V N 2023 *Sci. Bull.* **68** 2017

[12] Zhong H, Kompanets V O, Zhang Y, Kartashov Y V, Cao M, Li Y, Zhuravitskii S A, Skryabin N N, Dyakonov I V, Kalinkin A A, Kulik S P, Chekalin S V, and Zadkov V N 2024 *Light Sci. Appl.* **13** 264

[13] Huang B 2023 *Front. Phys.* **18** 13601

[14] He C, Zhao L, Zhang S, Zhou L, and Ma S 2025 *eLight* **5** 19

[15] Rechtsman M C, Zeuner J M, Plotnik Y, Lumer Y, Podolsky D, Dreisow F, Nolte S, Segev M, and Szameit A 2013 *Nature* **496** 196

[16] Peterson C W, Li T, Benalcazar W A, Hughes T L, and Bahl G 2020 *Science* **368** 1114

[17] Peterson C W, Li T, Jiang W, Hughes T L, and Bahl G 2021 *Nature* **589** 376

[18] Liu Y, Leung S, Li F F, Lin Z K, Tao X, Poo Y, and Jiang J H 2021 *Nature* **589** 381

[19] Wu L H and Hu X 2015 *Phys. Rev. Lett.* **114** 223901

[20] Ren B, Arkhipova A A, Zhang Y, Kartashov Y V, Wang H, Zhuravitskii S A, Skryabin N N, Dyakonov I V, Kalinkin A A, Kulik S P, Kompanets V O, Chekalin S V, and Zadkov V N 2023 *Light Sci. Appl.* **12** 194

[21] Kompanets V O, Feng S, Zhang Y, Kartashov Y V, Li Y, Zhuravitskii S A, Skryabin N N, Kireev A V, Dyakonov I V, Kalinkin A A, Shang C, Kulik S P, Chekalin S V, and Zadkov V N 2025 *Adv. Mater.* **37** 2500556

[22] Zhang B, Yan W, and Chen F 2025 *Adv. Photon.* **7** 034002

[23] Huang C, Kireev A V, Jiang Y, Kompanets V O, Shang C, Kartashov Y V, Zhuravitskii S A, Skryabin N N, Dyakonov I V, Kalinkin A A, Kulik S P, Ye F, and Zadkov V N 2025 *Commun. Phys.* **8** 451

[24] Wang Z, Meng Y, Yan B, Zhao D, Yang L, Chen J, Cheng M, Xiao T, Shum P P, Liu G G, Yang Y, Chen H, Xi X, Zhu Z X, Xie B, and Gao Z 2025 *Nat. Commun.* **16** 3122

[25] Qiu S, Hu J, Yang Y, Shang C, Liu S, and Cui T J 2025 *National Sci. Rev.* **12** nwaf137

[26] Ren B, Kartashov Y V, Maczewsky L J, Kirsch M S, Wang H, Szameit A, Heinrich M, and Zhang Y 2023 *Nanophoton.* **12** 3829

[27] Li M, Li C, Yan L, Li Q, Gong Q, and Li Y 2023 *Light Sci. Appl.* **12** 262

[28] Shi A, Peng Y, Jiang J, Peng Y, Peng P, Chen J, Chen H, Wen S, Lin X, Gao F, and Liu J 2024 *Laser Photon. Rev* **18** 2300956

[29] Arkhipova A A, Kartashov Y V, Ivanov S K, Zhuravitskii S A, Skryabin N N, Dyakonov I V, Kalinkin A A, Kulik S P, Kompanets V O, Chekalin S V, Ye F, Konotop V V, Torner L, and Zadkov V N 2023 *Phys. Rev. Lett.* **130** 083801

[30] Lu C, Gao Y, Cao X, Ren Y, Han Z, Cai Y, and Wen Z 2023 *Phys. Rev. B* **108** 014310

[31] Liu X and Zeng J 2024 *Front. Phys.* **19** 42201

[32] Li T T, Guo Z H, Wang X N, and Zhu Q 2025 *Front. Phys.* **20** 42201

[33] Peng R, Yang K, Fu Q, Chen Y, Wang P, Kartashov Y V, Konotop V V, and Ye F 2025 *eLight* **5** 16

[34] Jia H, Yang S, He J, Liu S, Chen H, Shang C, Ma S, Han P, Lee C H, Gao Z, Lai Y, and Cui T J 2025 arXiv: 2510.24463 [cond-mat.dis-nn]

[35] Lu C C, Yuan H Y, Zhang H Y, Zhao W, Zhang N E, Zheng Y J, Elshahat S, and Liu Y C 2022 *Chip* **1** 100025

[36] Leykam D, Xue H, Zhang B, and Chong Y D 2025 *Nat. Rev. Phys.* (in press)